

Cyclic Structural Transformations from Crystalline to Crystalline to Amorphous Phases and Magnetic Properties of a Mn(II)-Based Metal-Organic Framework

Han Geul Lee, Chang Seop Hong, Hyuna Jo, Sunhwi Eom, Dong Won Kang, Minjung Kang, Jeremy Hilgar, Jeffrey D. Rinehart, and Dohyun Moon

Cryst. Growth Des., **Just Accepted Manuscript** • DOI: 10.1021/acs.cgd.8b00064 • Publication Date (Web): 24 Apr 2018

Downloaded from <http://pubs.acs.org> on April 24, 2018

Just Accepted

“Just Accepted” manuscripts have been peer-reviewed and accepted for publication. They are posted online prior to technical editing, formatting for publication and author proofing. The American Chemical Society provides “Just Accepted” as a service to the research community to expedite the dissemination of scientific material as soon as possible after acceptance. “Just Accepted” manuscripts appear in full in PDF format accompanied by an HTML abstract. “Just Accepted” manuscripts have been fully peer reviewed, but should not be considered the official version of record. They are citable by the Digital Object Identifier (DOI®). “Just Accepted” is an optional service offered to authors. Therefore, the “Just Accepted” Web site may not include all articles that will be published in the journal. After a manuscript is technically edited and formatted, it will be removed from the “Just Accepted” Web site and published as an ASAP article. Note that technical editing may introduce minor changes to the manuscript text and/or graphics which could affect content, and all legal disclaimers and ethical guidelines that apply to the journal pertain. ACS cannot be held responsible for errors or consequences arising from the use of information contained in these “Just Accepted” manuscripts.



1
2
3
4 Cyclic Structural Transformations from Crystalline to
5
6
7 Crystalline to Amorphous Phases and Magnetic
8
9
10
11 Properties of a Mn(II)-Based Metal-Organic Framework
12
13
14
15
16
17
18
19

20 Han Geul Lee,^{†,‡} Hyuna Jo,^{†,‡} Sunhwi Eom,[†] Dong Won Kang,[†] Minjung Kang,[†] Jeremy Hilgar,[§]
21
22 Jeffrey D. Rinehart,[§] Dohyun Moon[⊥] and Chang Seop Hong^{*,†}
23
24
25
26
27
28

29 [†]*Department of Chemistry, Korea University, 145 Anam-ro, Seongbuk-gu, Seoul 02841, Republic of*
30
31 *Korea.*
32
33

34 [§]*Department of Chemistry and Biochemistry, University of California – San Diego, 9500 Gilman Drive,*
35
36 *Mail Code 0358, La Jolla, CA 92093-0358, USA.*
37
38
39

40 [⊥]*Beamline Division, Pohang Accelerator Laboratory, Pohang, Kyungbuk 790-784, Republic of Korea.*
41
42
43
44
45
46
47
48
49
50
51
52
53
54
55
56
57
58
59
60

1 **ABSTRACT:** A three-dimensional Mn(II) framework,
2 [Mn₂(H₂L)(L)_{0.5}(MeOH)(DEF)]·0.1MeOH·0.1DEF·1.4H₂O (**1**; H₄L = 2,3-dioxido-1,4-
3 benzenedicarboxylic acid), was synthesized under solvothermal conditions in
4 diethylformamide/methanol (DEF/MeOH), where the Mn centers adopt octahedral and unusual
5 pentagonal bipyramidal geometries. The ligand H₄L was subject to deprotonation to create μ₄-H₂L²⁻ and
6 μ₆-L⁴⁻ anionic bridges, leading to the construction of a coordination network. MeOH exchange process
7 of crystalline **1** allowed for another crystalline phase (**1a**), which reversibly returned to the original
8 crystalline state upon resolution in DEF/MeOH. After evacuation of **1a**, the amorphous phase **1b** was
9 irreversibly formed, followed by the restoration of the original phase **1** upon resolution in DEF/MeOH.
10 Consequently, this framework underwent cyclic structural transformations from the crystalline (**1**) to
11 crystalline (**1a**) to amorphous (**1b**) and back to crystalline (**1**) phase, which are unique transformations
12 for soft coordination networks. Magnetic measurements demonstrated that antiferromagnetic
13 interactions were operative between the Mn(II) ions, and were effectively mediated by the oxygen
14 moieties of the μ₆-L⁴⁻ bridge.
15
16
17
18
19
20
21
22
23
24
25
26
27
28
29
30
31
32
33
34
35
36
37
38
39
40
41
42
43
44
45
46
47
48
49
50
51
52
53
54
55
56
57
58
59
60

INTRODUCTION

1
2 Metal-organic frameworks (MOFs) are crystalline platforms that are characterized by high surface
3 area and porosity. Their applications include gas storage and separation, catalysis, proton conductivity,
4 sensing, drug delivery, and so on.¹⁻⁵ Although MOFs frequently exhibit structural rigidity, they are
5 flexible upon external stimuli such as host-guest interactions, photo- and thermo responses, and
6 pressure.⁶ Such structural flexibility emerges as a result of breathing, swelling, linker rotation, and
7 subnetwork displacement within the framework structure.
8
9

10
11 In terms of host-guest interactions, solvent molecules incorporated into the interior of the framework
12 trigger structural flexibility of the dynamic soft crystals. Substantial structural variations in soft
13 coordination networks are accompanied by changes in the ligand conformation and deformation of the
14 metal nodes when guest molecules enter or exit the pores of the framework.⁷⁻⁹ Solvent inclusion in or
15 removal from the framework often engenders single crystal-to-single crystal transformations.¹⁰⁻¹² The
16 structural dynamics in flexible coordination systems also promotes crystal-to-amorphous structural
17 conversions upon solvation-desolvation.¹³⁻¹⁶ Thus, most structural transformations involve reversible or
18 irreversible phase exchange between two crystalline states or between crystalline and amorphous states.
19 In fact, structural nonrigidity of soft frameworks is more diverse and even three states are mutually
20 transformable upon various sample treatments (solvent exchange, activation, and resolution, for
21 instance).¹⁷⁻¹⁹ In these examples, phase conversions from crystalline to another crystalline to other
22 crystalline states occur upon incorporation of guest solvent molecules into the frameworks or
23 elimination of the introduced solvent molecules. Based on these observations, it was envisioned that
24 more extensive framework dynamics could be achieved in association with the creation of new multiple
25 phases under different external conditions.
26
27

28
29 Herein, we report the synthesis, crystal structure, multi-structural flexibility, and magnetic properties
30 of the three-dimensional (3D) network of $[\text{Mn}_2(\text{H}_2\text{L})(\text{L})_{0.5}(\text{MeOH})(\text{DEF})]\cdot 0.1\text{MeOH}\cdot 0.1\text{DEF}\cdot 1.4\text{H}_2\text{O}$ (**1**;
31 $\text{H}_4\text{L} = 2,3\text{-dioxido-1,4-benzenedicarboxylic acid}$). This network exhibits significant structural flexibility
32 in connection with extensive cyclic conversions from one crystalline phase to another crystalline phase
33
34
35
36
37
38
39
40
41
42
43
44
45
46
47
48
49
50
51
52
53
54
55
56
57
58
59
60

to an amorphous phase to the original crystalline state during solvent inclusion and removal. It is remarkable that these phase transformations take place among three states, including an amorphous phase, which has not been demonstrated before to the best of our knowledge. Antiferromagnetic coupling occurs between the Mn(II) ions, mediated by the oxygen atoms of the organic ligand.

EXPERIMENTAL SECTION

Reagents. All chemicals and solvents used in the synthesis were of reagent grade and were used as received. All manipulations were performed under aerobic conditions.

2,3-Dioxido-1,4-benzenedicarboxylic acid (H₄L). 1,2,4-Trichlorobenzene (5 mL) was added to a mixture of pyrocatechol (1.00 g, 9.08 mmol) and KHCO₃ (2.91 g, 29.06 mmol), and the mixture was placed in a 23-mL autoclave. The bomb was sealed after adding dry ice (5.836 g, 132.6 mmol) and placed in an oven heated to 225 °C for 14 h. The resulting mixture was washed with diethyl ether by stirring for 30 min and collected by vacuum filtration. The crude product was dissolved in 600 mL of water by stirring for 30 min and filtered through a Celite® filter aid. Hydrochloric acid was slowly added to the solution until the pH reached 1–2. The precipitate was collected by filtration and washed with water. A beige color solid was obtained and dried at 70 °C. Yield = 73%. ¹H NMR (DMSO-*d*₆, 500 MHz) δ(ppm): 7.28(s). Anal. Calcd for C₈H_{7.9}O_{6.95} (H₄L·0.95H₂O): C, 44.64; H, 3.70. Found: C, 44.69; H, 3.72.

[Mn₂(H₂L)(L)_{0.5}(MeOH)(DEF)]·0.1MeOH·0.1DEF·1.4H₂O (1). MnCl₂·4H₂O (534.3 mg, 2.7 mmol) and H₄*o*-dobdc (178.3 mg, 0.9 mmol) were dissolved in a mixed solvent comprising *N,N*-diethylformamide (DEF)/MeOH (5/1, v/v, 9 mL) by sonication. The filtered brownish solution and hydrochloric acid (0.09 mL) were transferred to a 23-mL glass vial and sealed tightly. The vial was placed in an oven pre-heated to 120 °C for 1 day. The resulting solid was washed with DEF/MeOH (5/1, v/v, 120 mL) mixed solvent (mother liquor) and then with MeOH (30 mL). The solid was collected by filtration, followed by drying in Ar for 1 h, affording a brownish solid. Yield = 53%. Anal. Calcd. for C_{18.6}H_{24.3}Mn₂N_{1.1}O_{12.6}: C, 38.87; H, 4.26; N, 2.68. Found: C, 38.73; H, 3.92; N, 2.94.

Reversible Phase Conversion between 1 and 1a upon MeOH Exchange and DEF/MeOH

Resolution. **1** was soaked in MeOH for 5 days, where the solvent was refreshed every day. The solid was collected by filtration and Ar-dried for 1 h to produce the MeOH-exchange sample of $[\text{Mn}_2(\text{H}_2\text{L})(\text{L})_{0.5}(\text{MeOH})_2] \cdot 1.8\text{H}_2\text{O}$ (**1a**). Anal. Calcd. for $\text{C}_{14}\text{H}_{16.6}\text{O}_{12.8}$: C, 33.66; H, 3.35. Found: C, 33.74; H, 3.16. **1a** was immersed in DEF/MeOH (5/1, v/v) mixed solvent for 3 d, where the solvent was refreshed every day. The solid was collected by filtration, followed by drying in Ar for 1 h to give the regenerated sample of $[\text{Mn}_2(\text{H}_2\text{L})(\text{L})_{0.5}(\text{MeOH})_{1.28}(\text{DEF})_{0.72}] \cdot 1.1\text{H}_2\text{O}$. Anal. Calcd. for $\text{C}_{16.88}\text{H}_{20.24}\text{Mn}_2\text{N}_{0.72}\text{O}_{12.1}$: C, 37.78; H, 3.80; N 1.88. Found: C, 37.48; H, 3.58; N, 1.89. These processes were monitored by powder X-ray diffraction (PXRD) and infrared (IR) analyses.

Phase Transformation from Crystalline 1a to Amorphous 1b upon Activation. **1a** was evacuated for 1 h to generate the activated solid $[\text{Mn}_2(\text{H}_2\text{L})(\text{L})_{0.5}] \cdot 2.4\text{H}_2\text{O} \cdot 0.6\text{MeOH}$ (**1b**). Anal. Calcd. for $\text{C}_{12.6}\text{H}_{12.2}\text{Mn}_2\text{O}_{12}$: C, 32.51; H, 2.64. Found: C, 32.67; H, 2.86. This process was monitored by PXRD and IR.

Phase Transformation from Amorphous 1b to Crystalline 1 upon DEF/MeOH Resolution. **1b** was soaked in DEF/MeOH (5/1, v/v) mixed solvent for 3 d, where the solvent was refreshed every day. Filtration and Ar drying of the resulting solid afforded the resolved phase of $[\text{Mn}_2(\text{H}_2\text{L})(\text{L})_{0.5}(\text{MeOH})_{0.5}(\text{DEF})_{0.82}(\text{H}_2\text{O})_{0.68}] \cdot 1.72\text{H}_2\text{O}$. Anal. Calcd. for $\text{C}_{16.6}\text{H}_{20.82}\text{Mn}_2\text{N}_{0.82}\text{O}_{12.72}$: C, 36.57; H, 3.85; N 2.11. Found: C, 36.19; H, 3.45; N, 2.48. This process was monitored by PXRD and IR.

Physical Measurements. Proton nuclear magnetic resonance spectra (^1H NMR) were recorded with a 500 MHz NMR spectrometer. Infrared spectra were obtained with an ATR module using a Nicolet iS10 FT-IR spectrometer. Powder XRD (PXRD) patterns were recorded on a Rigaku Ultima III diffractometer using Cu-K_α ($\lambda = 1.5406 \text{ \AA}$) radiation, with a scan speed of $2^\circ/\text{min}$ and a step size of 0.01° . Elemental analyses for C, N, and H were performed at the Elemental Analysis Service Center of Sogang University. Gas sorption measurements were carried out on a ASAP2020 instrument at 77 K

(N₂). Magnetic data for **1** were acquired with a Quantum Design SQUID susceptometer. Diamagnetic corrections for **1** were estimated from Pascal's Tables.

Crystallographic Structure Determination. X-ray data for a single crystal of **1** were acquired with a cryoloop, where the crystal was mounted on a goniometer head under a cold stream of liquid nitrogen. The diffraction data were acquired by applying synchrotron radiation on a 2D SMC MX ADSC Quantum-210 detector with a silicon (111) double-crystal monochromator at the Pohang Accelerator Laboratory, Korea. The ADSC Quantum-210 ADX program (Ver. 1.92) was used for data collection, while HKL3000 (Ver. 0.98.699) was used for cell refinement, reduction, and absorption correction. The structure was solved by direct methods and refined by full-matrix least-squares analysis using anisotropic thermal parameters for non-hydrogen atoms with the SHELXTL program. The lattice solvent molecules in **1** were significantly disordered and could not be modeled properly, thus the program SQUEEZE, a part of the PLATON crystallographic software package, was used to calculate the solvent disorder area and remove its contribution to the overall intensity data. All hydrogen atoms, except for those bound to water molecules, were calculated at idealized positions and refined with the riding model. Crystal data for **1**: empirical formula = C₃₁H₄₉Mn₄NO₂₂, *M_r* = 1007.47, monoclinic, space group C2/c, *a* = 21.180(4) Å, *b* = 11.551(2) Å, *c* = 19.602(4) Å, *β* = 106.06(3)°, *V* = 4608.4(16) Å³, *Z* = 4, *D*_{calc} = 1.452 g cm⁻³, *μ* = 1.146 mm⁻¹, 21520 reflections collected, 6287 unique (*R*_{int} = 0.0514), *R*1 = 0.0648, *wR*2 = 0.1752 [*I* > 2σ(*I*)]. CCDC 1814445 (**1**) contains the supplementary crystallographic data for this paper. These data can be obtained free of charge from The Cambridge Crystallographic Data Centre via www.ccdc.cam.ac.uk/data_request/cif.

RESULTS AND DISCUSSION

Description of Crystal Structure. Two types of Mn atoms (Mn1 and Mn2) are present in the asymmetric unit of the crystal structure (Figure 1a). Mn1 is surrounded by seven oxygens from H₂L²⁻, L⁴⁻, and a DEF molecule, whereas Mn2 adopts a distorted octahedral geometry consisting of six oxygens from H₂L²⁻, L⁴⁻, and a MeOH molecule (Figure S1). To determine the exact coordination environment

1 around heptacoordinate Mn1, we performed a continuous shape measures (CShM) analysis.²⁰⁻²² The
2 ideal geometry for heptacoordination involves a pentagonal bipyramid (PBPY, D_{5h}), a capped
3 octahedron (COC, C_{3v}), and a capped trigonal prism (CTPR, C_{2v}). We calculated the S_X ($X =$ PBPY,
4 COC, CTPR) terms, resulting in values of 1.386, 6.497, and 5.525, respectively. From the obtained
5 values, we concluded that Mn1 adopts a distorted pentagonal bipyramidal geometry, which is rarely
6 encountered in coordination chemistry, except in six-fold coordination (Figure S2).
7
8
9
10
11
12

13
14 In terms of the structural parameters, the Mn1-O lengths range from 2.141(3) to 2.488(2) Å, while the
15 Mn2-O distances span from 2.103(2) to 2.192(2) Å. The bond angles of Mn-O-Mn are 99.54(9)° for
16 Mn1a-O1a-Mn2, 110.37(9)° for Mn1a-O3-Mn2, and 117.82(10)° for Mn1-O2-Mn2. The Mn-Mn
17 distances bridged by the carboxylates and oxygen atoms are 3.7876(7) Å for Mn1-Mn2 and 3.5645(6) Å
18 for Mn2-Mn1a. In the Mn1a-Mn2 connection, the Mn1a atom is linked to Mn2 *via* two carboxylates and
19 one oxygen (O2) atom.
20
21
22
23
24
25
26

27 The extended structure showing the evolution of the one-dimensional chain is illustrated in Figure 1b.
28 An octahedron connects two adjacent pentagonal bipyramids *via* corner or edge sharing to form an AB
29 stacking sequence along the chain direction. In the chain, there are two types of bridging ligands, i.e.,
30 H_2L^{2-} and L^{4-} . H_2L^{2-} simultaneously binds four Mn atoms with two unprotonated hydroxyl groups,
31 serving as a μ_4 -bridge, whereas L^{4-} can act as a μ_6 -bridge to connect six Mn atoms (Figure S3). Notably,
32 the binding mode of L^{4-} is unique and has never been demonstrated in framework structures to the best
33 of our knowledge.^{23, 24} An additional notable feature is that such direct incorporation of the H_2L^{2-} type
34 ligand into a framework is unprecedented because only post-synthetic exchange or post-synthetic
35 deprotection of a pristine framework with H_4L could lead to the construction of an architecture with
36 H_2L^{2-} .^{23, 24} The bridging μ_6 - L^{4-} ligands link Mn atoms to generate one-dimensional (1D) chains and
37 subsequently form a two-dimensional (2D) sheet (Figure 1c). The sheets are interconnected by H_2L^{2-}
38 bridges to give a 3D structure (Figure 1d and S4). Two types of solvent molecules (MeOH and DEF)
39 coordinated to Mn centers are located in the square window toward the pore. In the pore, one DEF
40 molecule takes up two sites with an occupancy of 0.5 (Figure 1e). To assess the topology of a
41
42
43
44
45
46
47
48
49
50
51
52
53
54
55
56
57
58
59
60

1 framework, the Mn₂ dimer (Mn1 and Mn2b) is represented by a node, and the organic linkers of H₂L²⁻
2 and L⁴⁻ are denoted by a stick. The 3D network features a five-connected hexagonal BN net with a point
3 symbol of {4⁶.6⁴} (Figure S5).²⁵
4
5

6
7 **Phase Transformations.** The PXRD data of as-synthesized **1** were acquired and compared with the
8 simulated pattern (Figure 2). The phase purity of **1** was confirmed based on the coincidence of the
9 experimental and simulated patterns. To examine the structural transformability, **1** was immersed in
10 MeOH for five days at room temperature. The solvent was refreshed every day to ensure the complete
11 replacement of DEF with MeOH. The PXRD profile of the MeOH-exchanged sample (**1a**) was different
12 from that of **1**, which indicates the formation of a new crystalline phase. While the colors of **1** and **1a**
13 were almost identical, the single crystallinity was almost lost in **1a** as confirmed by scanning electron
14 microscopy (Figure S6). The cell dimensions of **1** shrank upon soaking in MeOH, where the peaks in the
15 profile of **1a** were shifted to higher 2θ angles. In the IR spectrum of **1**, the peak at 1644 cm⁻¹ is assigned
16 to the C=O stretching band of the DEF molecule (Figure 3). This band disappeared after immersion of **1**
17 in MeOH, indicating the removal of DEF during the MeOH exchange process, as corroborated by
18 elemental analysis. The pristine phase of **1** was restored by soaking **1a** in DEF/MeOH for three days, as
19 confirmed by PXRD. The presence of the C=O peak in the IR spectrum after resolution indicates the
20 incorporation of DEF into the framework of resolvated **1**. Furthermore, **1a** was evacuated at several
21 temperatures (40, 60, 120, and 150 °C) to remove the solvent molecules (Figure S7). After 1 h of
22 evacuation, the framework collapsed, even at room temperature, to afford the activated phase **1b**. The
23 PXRD pattern of **1b** showed no distinct peaks, demonstrating structural amorphization during the
24 activation process. A crystal-to-amorphous conversion occurs when the long-range structural order of
25 the crystalline phase is lost.^{13, 26} Such structural disintegration is triggered by elimination of guest or
26 coordinated molecules from the coordination system. Thus, herein, the pore structure was disorganized
27 as elucidated from the 77 K N₂ sorption isotherm, where no adsorption was observed (Figure S8). The
28 resolution of **1b** was attempted by immersing the sample in MeOH for five days. Under this solvation
29 condition, the MeOH-exchanged phase **1a** was not recovered, but the amorphous state **1b** was
30
31
32
33
34
35
36
37
38
39
40
41
42
43
44
45
46
47
48
49
50
51
52
53
54
55
56
57
58
59
60

maintained, as demonstrated by the PXRD pattern (Figure S9). This result implies that the conversion from **1b** to **1a** is irreversible. To probe the role of the solvent molecules in the crystallization process, **1b** was soaked in a mixed solvent of DEF and MeOH. Notably, as long as DEF was introduced into the mixed solvent system, the original crystalline phase of **1** was reformed. This is in contrast with the MeOH solvation case. It appears that the inclusion of DEF molecules into the framework plays a key role in this amorphous-to-crystalline phase transformation. From the crystal structure (Figure 1e), the DEF molecules are bonded to Mn centers and located in the square channels. The recovery of the crystalline state seems to be initiated by DEF coordination and pore packing in the framework structure.

Framework flexibility triggered by removal and inclusion of solvent molecules commonly occurs in concert with transformations between two crystalline states or between crystalline and amorphous phases.^{13-16, 27} Furthermore, mutual interconversion among three crystalline states after treatment of samples with different solvents and after evacuation has been reported.^{17-19, 28} Notably, the present framework undergoes conversion from one crystalline state (**1**) to another crystalline state (**1a**) to an amorphous phase (**1b**) and eventually back to the original crystalline state (**1**). Thus, such multi-step transformations including an amorphous phase are unique among solvent-induced phase transitions because only phase changes between two states and among three crystalline states have been commonly demonstrated to date.

Magnetic Properties. The magnetic data for **1** were collected as a function of the temperature at $H_{dc} = 1000$ Oe (Figure 4a). The $\chi_m T$ value per Mn^{II} ion was $4.27 \text{ cm}^3 \text{ K mol}^{-1}$ at 300 K, which is somewhat lower than the value ($4.38 \text{ cm}^3 \text{ K mol}^{-1}$) calculated using the parameters $S = 5/2$ and $g = 2$. As the temperature decreased, the $\chi_m T$ product underwent a slow downturn and then rapidly declined to $0.39 \text{ cm}^3 \text{ K mol}^{-1}$ at 2 K.

To understand the magnetic coupling between the paramagnetic centers, we probed the metric parameters of the structure (Figure 1a). In the bridging pathway of Mn1a-O1a-Mn2, the Mn1a-O1a bond length is $2.488(2) \text{ \AA}$, which is much longer than the Mn2-O1a bond length of $2.174(2) \text{ \AA}$. The longer Mn1a-O1a bond length could make the magnetic contribution of the Mn1a-O1a-Mn2 route negligible. In

1 comparison, the Mn1a-O3-Mn2 path has shorter bond length parameters of Mn1a-O3 = 2.209(2) Å and
2 Mn2-O3 = 2.132(2) Å, thereby generating an effective magnetic pathway. In this route, the Mn1a-O3-
3 Mn2 bond angle is 110.37(9)°. Regarding the Mn1 and Mn2 centers, the two carboxylate bridges
4 provide longer magnetic pathways through three atoms. Mn1-O2-Mn2 bridged by one oxygen atom
5 provides a more efficient path. The relevant bond distances are 2.303(2) Å for Mn1-O2 and 2.119(2) Å
6 for Mn2-O2, and the bond angle of Mn1-O2-Mn2 is 117.82(10)°. The metric parameters of the Mn1-O2-
7 Mn2 route are similar to the corresponding counterparts in the Mn1a-O3-Mn2 linkage. Thus, these two
8 magnetic routes are considered effective pathways for magnetic coupling. From the similar bond lengths
9 and angles, the two magnetic paths are reasonably assumed to give an identical coupling constant.

10
11
12
13
14
15
16
17
18
19
20
21 On the basis of the structural analysis, we fitted the magnetic data of **1** to an infinite uniform chain
22 model with the spin Hamiltonian $H = -J\sum S_i \cdot S_{i+1}$. To include interchain interactions, the mean-field
23 approximation (zj') was taken into account in the fitting process. The best result afforded values of $J = -$
24 1.98 cm^{-1} and $zj' = -0.2 \text{ cm}^{-1}$ with g fixed at 2.00. We also tried to analyze the magnetic data with two J
25 (J_1 and J_2) systems based on $H = -J_1\sum S_{2i} \cdot S_{2i+1} - J_2\sum S_{2i+1} \cdot S_{2i+2}$.^{29, 30} A best simulation resulted in
26 parameters almost identical to the one J system. The negative J value suggests the existence of
27 antiferromagnetic coupling between the Mn^{II} ions. The experimental field-dependent magnetization data
28 were far below the saturation value expected from the Brillouin equation, indicating a paramagnetic
29 state with $S = 5/2$ (Figure 4b). This indicates that the Mn spins are antiferromagnetically coupled along
30 the chain. The overall magnetic trend of **1a** is similar to that of **1**, as shown in Figure S10.

31 32 33 34 35 36 37 38 39 40 41 42 43 44 45 46 **CONCLUSIONS**

47
48 A 3D Mn(II) framework incorporating octahedral and uncommon pentagonal bipyramidal geometries
49 around Mn was prepared. The organic ligands act as a μ_4 -bridge or a μ_6 -bridge depending on the degree
50 of deprotonation of the ligand, leading to the construction of a network structure. The framework is
51 highly flexible and uniquely transformable from crystalline to crystalline to amorphous to crystalline
52 phases upon solvent exchange, activation, and resolution. The magnetic measurements indicate that
53
54
55
56
57
58
59
60

antiferromagnetic interactions between the Mn spins are operative through the oxygen species of the μ_6 -bridge.

ASSOCIATED CONTENT

Supporting Information. X-ray crystallographic files in CIF format, additional structural data for the complexes. This material is available free of charge via the Internet at <http://pubs.acs.org>.

AUTHOR INFORMATION

Corresponding Author

*E-mail: cshong@korea.ac.kr

Author Contributions

‡These authors contributed equally.

ACKNOWLEDGMENT

This work was supported by the Korea CCS R&D Center (KCRC) grant funded by the Korean government (the Ministry of Science, ICT, & Future Planning (MSIP)) (NRF-2014M1A8A1049253), the Basic Science Research Program (NRF-2015R1A2A1A10055658), the Priority Research Centers Program (NRF-20100020209), and PAL.

REFERENCES

- (1) Yu, J.; Xie, L. H.; Li, J. R.; Ma, Y.; Seminario, J. M.; Balbuena, P. B., CO₂ Capture and Separations Using MOFs: Computational and Experimental Studies. *Chem. Rev.* **2017**, *117*, 9674-9754.
- (2) Rogge, S. M. J.; Bavykina, A.; Hajek, J.; Garcia, H.; Olivos-Suarez, A. I.; Sepu'lveda-Escribano, A.; Vimont, A.; Clet, G.; Bazin, P.; Kapteijn, F.; Daturi, M.; Ramos-Fernandez, E. V.; Xamena, F. X. L. s. i.; Speybroeck, V. V.; Gascon, J., Metal-organic and covalent organic frameworks as single-site catalysts. *Chem. Soc. Rev.* **2017**, *46*, 3134-3184.
- (3) Ramaswamy, P.; Wong, N. E.; Shimizu, G. K., MOFs as proton conductors--challenges and opportunities. *Chem. Soc. Rev.* **2014**, *43*, 5913-5932.
- (4) Lustig, W. P.; Mukherjee, S.; Rudd, N. D.; Desai, A. V.; Li, J.; Ghosh, S. K., Metal-organic frameworks: functional luminescent and photonic materials for sensing applications. *Chem. Soc. Rev.* **2017**, *46*, 3242-3285.
- (5) Horcajada, P.; Gref, R.; Baati, T.; Allan, P. K.; Maurin, G.; Couvreur, P.; Ferey, G.; Morris, R. E.; Serre, C., Metal-organic frameworks in biomedicine. *Chem. Rev.* **2012**, *112*, 1232-1268.
- (6) Schneemann, A.; Bon, V.; Schwedler, I.; Senkovska, I.; Kaskel, S.; Fischer, R. A., Flexible metal-organic frameworks. *Chem. Soc. Rev.* **2014**, *43*, 6062-6096.

- (7) Serre, C.; Millange, F.; Thouvenot, C.; Nogue`s, M.; Marsolier, G. r.; Loue`r, D.; Fe`rey, G. r., Very Large Breathing Effect in the First Nanoporous Chromium(III)-Based Solids: MIL-53 or $\text{Cr}^{\text{III}}(\text{OH}) \cdot \{\text{O}_2\text{C}-\text{C}_6\text{H}_4-\text{CO}_2\} \cdot \{\text{HO}_2\text{C}-\text{C}_6\text{H}_4-\text{CO}_2\text{H}\}_x \cdot \text{H}_2\text{O}_y$. *J. Am. Chem. Soc.* **2002**, *124*, 13519-13526.
- (8) Seo, J.; Bonneau, C.; Matsuda, R.; Takata, M.; Kitagawa, S., Soft secondary building unit: dynamic bond rearrangement on multinuclear core of porous coordination polymers in gas media. *J. Am. Chem. Soc.* **2011**, *133*, 9005-9013.
- (9) Henke, S.; Schneemann, A.; Wutscher, A.; Fischer, R. A., Directing the breathing behavior of pillared-layered metal-organic frameworks via a systematic library of functionalized linkers bearing flexible substituents. *J. Am. Chem. Soc.* **2012**, *134*, 9464-9474.
- (10) Tang, S. F.; Hou, X.; Liu, D.; Zhao, X., Fabrication of New Uranyl Phosphonates by Varying Quaternary Ammonium Cation: Synthesis, Structure, Luminescent Properties, and Single-Crystal to Single-Crystal Transformation. *Inorg. Chem.* **2017**, *56*, 14524-14532.
- (11) Spirkel, S.; Grzywa, M.; Reschke, S.; Fischer, J. K. H.; Sippel, P.; Demeshko, S.; Krug von Nidda, H. A.; Volkmer, D., Single-Crystal to Single-Crystal Transformation of a Nonporous Fe(II) Metal-Organic Framework into a Porous Metal-Organic Framework via a Solid-State Reaction. *Inorg. Chem.* **2017**, *56*, 12337-12347.
- (12) Hou, J.-J.; Li, X.-Q.; Gao, P.; Sun, H.-Q.; Zhang, X.-M., Tunability in Metal Coordination Sphere, Ligand Coordination Mode, Network Topology, and Magnetism via Stepwise Dehydration Induced Single-Crystal to Single-Crystal Transformation. *Cryst. Growth Des.* **2017**, *17*, 3724-3730.
- (13) Lim, K. S.; Ryu, D. W.; Lee, W. R.; Koh, E. K.; Kim, H. C.; Hong, C. S., Reversible crystal-to-amorphous structural conversion in the single end-on azide-bridged Co(II) complex: concomitant color and magnetic modulations. *Chem. Eur. J.* **2012**, *18*, 11541-11544.
- (14) Sun, R.; Li, Y.-Z.; Bai, J.; Pan, Y., Synthesis, Structure, Water-Induced Reversible Crystal-to-Amorphous Transformation, and Luminescence Properties of Novel Cationic Spacer-Filled 3D Transition Metal Supramolecular Frameworks from N,N',N'' -Tris(carboxymethyl)-1,3,5-benzenetricarboxamide. *Cryst. Growth Des.* **2007**, *7*, 890-894.
- (15) Matoga, D.; Gil, B.; Nitek, W.; Todd, A. D.; Bielawski, C. W., Dynamic 2D manganese(ii) isonicotinate framework with reversible crystal-to-amorphous transformation and selective guest adsorption. *Cryst. Eng. Comm.* **2014**, *16*, 4959-4962.
- (16) Kang, G.; Jeon, Y.; Lee, K. Y.; Kim, J.; Kim, T. H., Reversible Luminescence Vapochromism and Crystal-to-Amorphous-to-Crystal Transformations of Pseudopolymorphic Cu(I) Coordination Polymers. *Cryst. Growth Des.* **2015**, *15*, 5183-5187.
- (17) Park, J. H.; Lee, W. R.; Kim, Y.; Lee, H. J.; Ryu, D. W.; Phang, W. J.; Hong, C. S., Interpenetration Control, Sorption Behavior, and Framework Flexibility in Zn(II) Metal-Organic Frameworks. *Cryst. Growth Des.* **2014**, *14*, 699-704.
- (18) Jeong, E.; Lee, W. R.; Ryu, D. W.; Kim, Y.; Phang, W. J.; Koh, E. K.; Hong, C. S., Reversible structural transformation and selective gas adsorption in a unique aqua-bridged Mn(II) metal-organic framework. *Chem. Commun.* **2013**, *49*, 2329-2331.
- (19) Kim, Y.; Song, J. H.; Lee, W. R.; Phang, W. J.; Lim, K. S.; Hong, C. S., Reversible Structural Flexibility and Sensing Properties of a Zn(II) Metal-Organic Framework: Phase Transformation between Interpenetrating 3D Net and 2D Sheet. *Cryst. Growth Des.* **2014**, *14*, 1933-1937.
- (20) Pinsky, M.; Avnir, D., Continuous Symmetry Measures. 5. The Classical Polyhedra. *Inorg. Chem.* **1998**, *37*, 5575-5582.
- (21) Casanova, D.; Cirera, J.; Lluell, M.; Alemany, P.; Avnir, D.; Alvarez, S., Minimal Distortion Pathways in Polyhedral Rearrangements. *J. Am. Chem. Soc.* **2004**, *126*, 1755-1763.
- (22) Cirera, J.; Ruiz, E.; Alvarez, S., Shape and spin state in four-coordinate transition-metal complexes: the case of the d(6) configuration. *Chem. Eur. J.* **2006**, *12*, 3162-3167.
- (23) Fei, H.; Shin, J.; Meng, Y. S.; Adelhardt, M.; Sutter, J.; Meyer, K.; Cohen, S. M., Reusable oxidation catalysis using metal-monocatecholato species in a robust metal-organic framework. *J. Am. Chem. Soc.* **2014**, *136*, 4965-4673.

- 1 (24) Lee, Y.; Kim, S.; Fei, H.; Kang, J. K.; Cohen, S. M., Photocatalytic CO₂ reduction using visible
2 light by metal-monocatecholato species in a metal–organic framework. *Chem. Commun.* **2015**, *51*,
3 16549-16552.
- 4 (25) Blatov, V. A.; Shevchenko, A. P., *TOPOS (Ver. 4.0)* **2011**, Samara State University, Russia.
- 5 (26) Tian, C. B.; Chen, R. P.; He, C.; Li, W. J.; Wei, Q.; Zhang, X. D.; Du, S. W., Reversible crystal-
6 to-amorphous-to-crystal phase transition and a large magnetocaloric effect in a spongelike metal organic
7 framework material. *Chem. Commun.* **2014**, *50*, 1915-1917.
- 8 (27) Lim, K. S.; Song, J. H.; Kang, D. W.; Kang, M.; Eom, S.; Koh, E. K.; Hong, C. S., Reversible
9 crystal-to-amorphous structural transformations and magnetic variations in single end-on azide-bridged
10 M(II) (M = Mn, Ni) coordination polymers. *Dalton Trans.* **2017**.
- 11 (28) Park, M. K.; Lim, K. S.; Park, J. H.; Song, J. H.; Kang, D. W.; Lee, W. R.; Hong, C. S., Two-
12 and three-dimensional Zn(II) coordination polymers constructed from mixed ligand systems:
13 interpenetration, structural transformation and sensing behavior. *CrystEngComm* **2016**, *18*, 4349-4358.
- 14 (29) Cortés, R.; Drillon, M.; Solans, X.; Lezama, L.; Rojo, T. f., Alternating Ferromagnetic-
15 Antiferromagnetic Interactions in a Manganese(II)-Azido One-Dimensional Compound:
16 [Mn(bipy)(N₃)₂]. *Inorg. Chem.* **1997**, *36*, 667-683.
- 17 (30) Wang, Y. Q.; Jia, Q. X.; Wang, K.; Cheng, A. L.; Gao, E. Q., Diverse Manganese(II)
18 Coordination Polymers with Mixed Azide and Zwitterionic Dicarboxylate Ligands: Structure and
19 Magnetic Properties. *Inorg. Chem.* **2010**, *49*, 1551-1560.
20
21
22
23
24
25
26
27
28
29
30
31
32
33
34
35
36
37
38
39
40
41
42
43
44
45
46
47
48
49
50
51
52
53
54
55
56
57
58
59
60

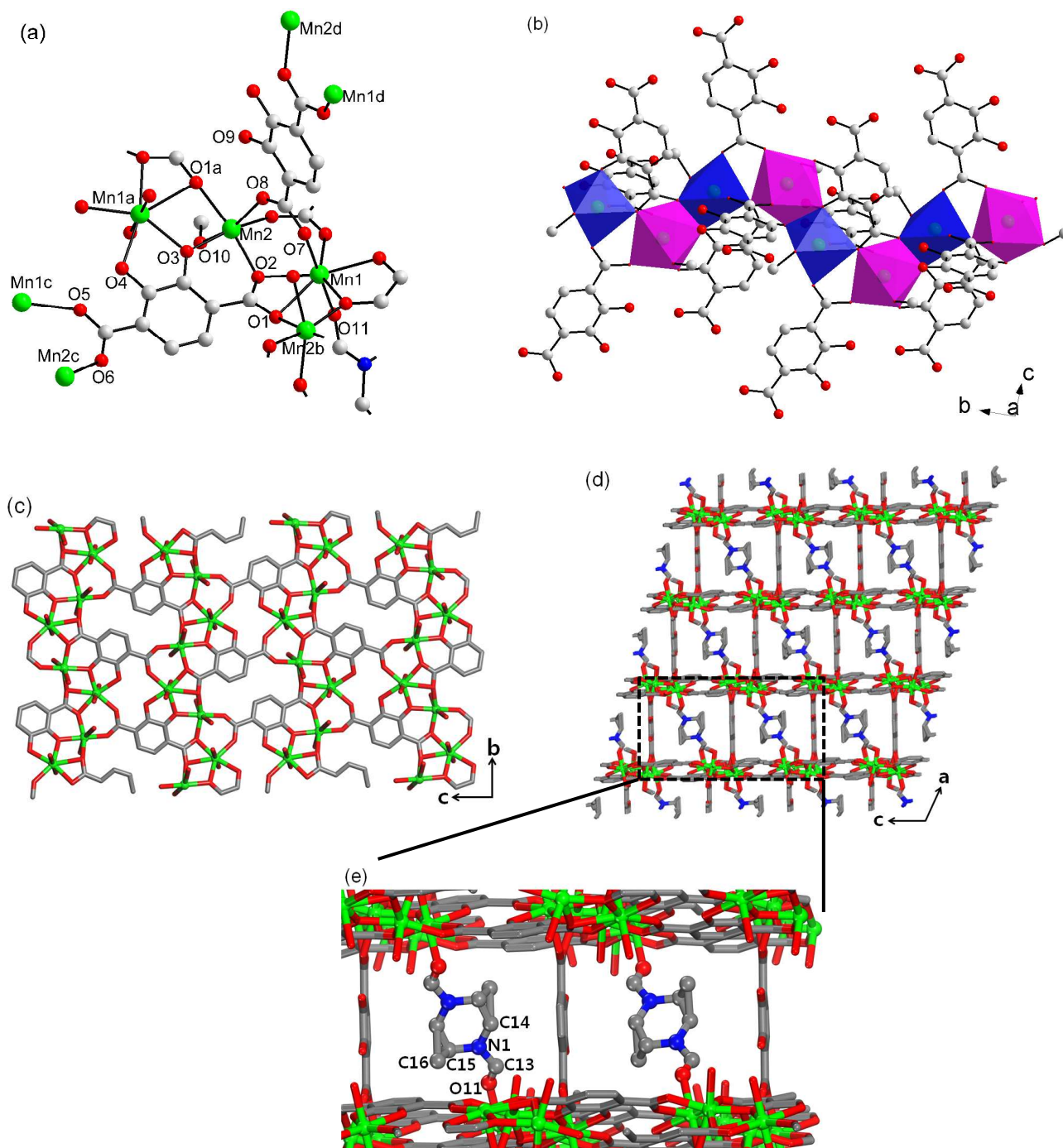


Figure 1. (a) Structure of **1** showing Mn coordination and binding modes of two types of organic ligands (L^{4-} and H_2L^{2-}). (b) 1D chain structure along the *b* axis showing two types of Mn coordination spheres. Blue polyhedron indicates a distorted octahedron for Mn2 and pink polyhedron denotes a distorted pentagonal bipyramid for Mn1. (c) 2D sheet formed by L^{4-} in the *bc* plane. (d) 3D network constructed by the 2D sheet in (c) and the intersheet connection of H_2L^{2-} and DEF ligands. (e) Enlargement of the dotted box in (d) detailing the intersheet disposition of DEF molecules with occupancy of 0.5.

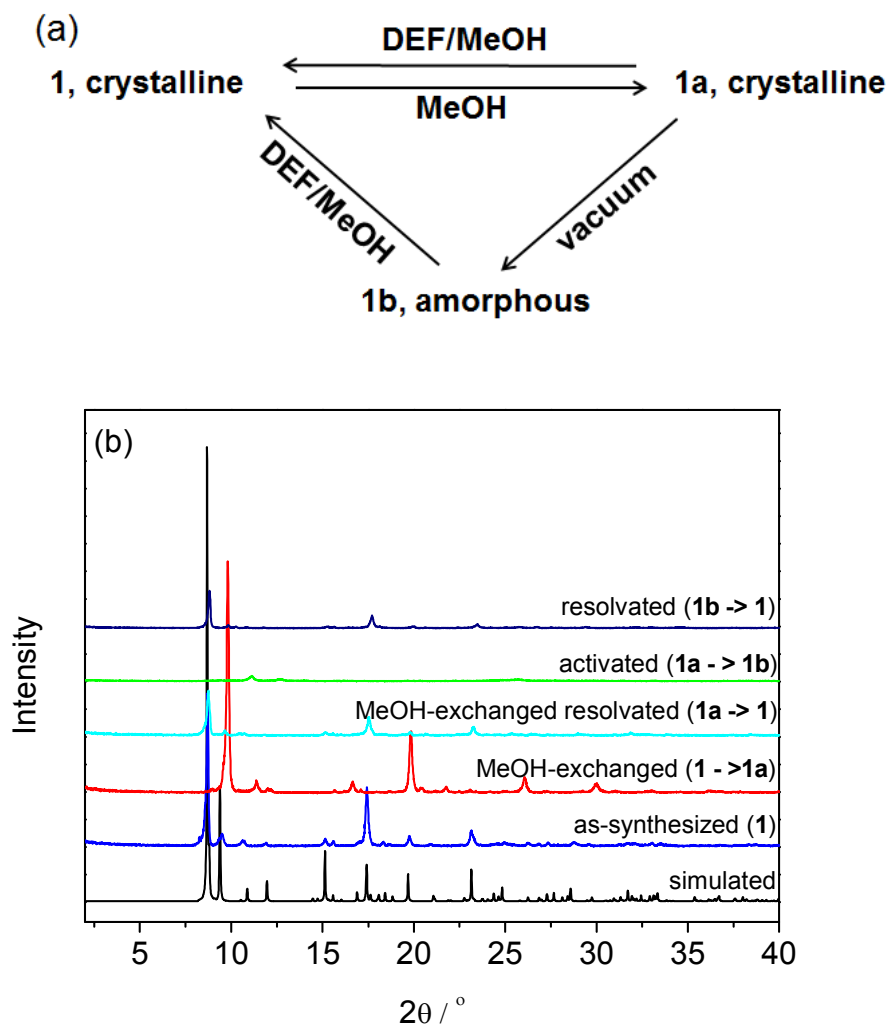


Figure 2. (a) Schematic representation of the reversible structural transformations among **1**, MeOH exchanged, and activated samples. (b) PXRD profiles of the as-synthesized, MeOH-exchanged, activated, and resoluted samples.

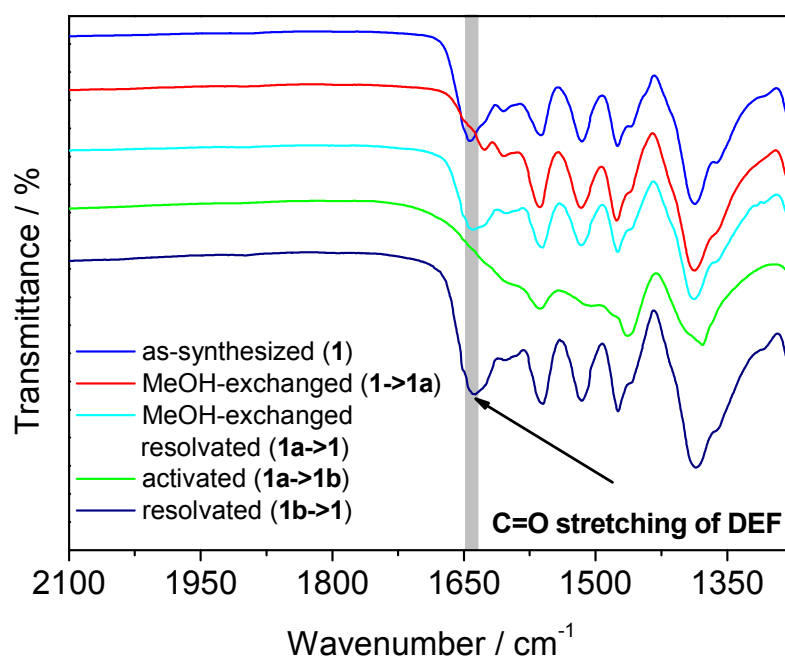


Figure 3. IR spectroscopic data for as-synthesized, MeOH-exchanged, activated, and resolvated samples.

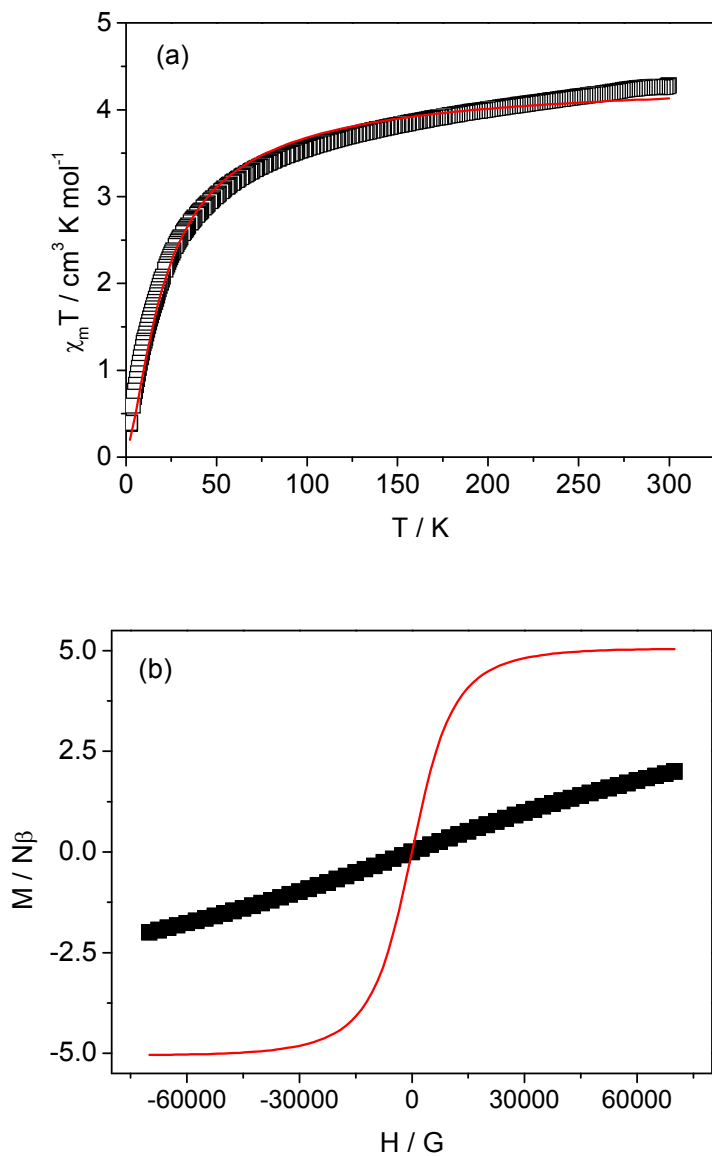


Figure 4. (a) Plot of $\chi_m T$ versus T of **1** in temperature range of 2 to 300 K. The solid line indicates the fitted result. (b) Field-dependence of the magnetization at 1.8 K. The solid line is the Brillouin curve for the uncoupled Mn(II) ion.

Synopsis

Cyclic Structural Transformations from Crystalline to Crystalline to Amorphous Phases and Magnetic Properties of a Mn(II)-Based Metal-Organic Framework

Han Geul Lee, Hyuna Jo, Sunhwi Eom, Dong Won Kang, Minjung Kang, Jeremy Hilgar, Jeffrey D.

Rinehart, Dohyun Moon and Chang Seop Hong

A three-dimensional Mn(II) metal-organic framework exhibits substantial structural flexibility associated with phase transformations from crystalline to crystalline to amorphous states.

